Observation of the effect of soil-structure boundaries using transparent soil technology

Guo Yu[1], *Yubo* Li[2], *Ying* Cui[1#] and *Lei* He[2]

[1]*Department of Civil Engineering, Yokohama National University, Yokohama, Japan*
[2]*School of Civil Engineering, Southeast University, Nanjing, China*
[#]*Corresponding author: sai-ei-mx@ynu.ac.jp*

ABSTRACT

The predominance of water flow at strata boundaries often triggers dam and levee failures. However, research on the porosity and water flow at soil-structure boundaries is insufficient despite the fact that the fact that their significant influence on water flows through soil is due to high porosity caused by compaction difficulties in the boundary region. Additionally, observing the interior of soil by conventional experimental methods is challenging, making it difficult to precisely determine the exact differences between the boundary area and surrounding grounds. Therefore, transparent soil techniques were employed to investigate the interior of the soil and the impact of soil-structure boundaries on flow path formation. The experiment identified two critical properties at the soil-structure boundary: relatively high porosity and the maximum average velocity of the fluid during permeability, both occurring at the interface. The good connectivity of the pores at the boundary is due to the barrier effect of the flat wall, which causes water to flow vertically upward along the boundary. In contrast, water flows meanderingly upward in the interior area of the soil, resulting in a two-dimensional movement at the boundary compared to a three-dimensional movement in the interior of the soil.

Keywords: seepage; soil-structure interface; transparent soil; PIV.

1. Introduction

The embankment dam is one of the most widely used water-retaining structures. According to statistics, embankment dam accounts for more than 70% of the world's high dams over 100 meters. Once the embankment dam fails, it will cause a massive loss of life and property in the downstream area, so it is essential to study the failure mechanism and failure process of the embankment dam.

The main structure of the embankment dam is composed of soil and stone, but it also contacts with other materials, such as the concrete cut-off wall, culvert, and bedrock. Due to different material properties, the soil-structure interface is more likely to be damaged than the soil interior, and this interface is also an accident-prone area (Luo et al. 2013). In 1976, the Teton Dam in Idaho, USA, was damaged. The cause of the accident was that the soil in the direct contact part between the clay core and the bedrock was eroded (Independent panel to review the cause of Teton dam failure 1976). In 1987, after the water level of Xizhaitang Reservoir in Beijing, China, dropped, two collapse pits were found on the upstream dam slope. The investigation showed that the cause of the accident was water leakage at the joints of the cut-off wall, which caused erosion of the soil in contact with the cut-off wall (Ru and Niu 2001). In 2004, the Bayi Reservoir in Xinjiang, China, broke due to the seepage failure between the newly built flood discharge culvert and the dam body (Jie Liu 2004).

Figure 1. Teton dam was destroyed (Independent panel to review the cause of Teton dam failure 1976).

To explore the causes of soil failure at the soil-structure interface, many scholars have studied its structural characteristics and failure mechanism. In terms of structural characteristics, it is mainly to explore the change of soil porosity from the interface to the interior. Some scholars simplified the problem by using spherical particles to replace soil particles. Mueller (1992) measured the porosity at various positions of spherical particles of identical size via X-ray and discovered that the porosity is highest at the interface between the particles and the side wall. Mueller (1997) determined the porosity variation pattern in spherical particles of the same size using four numerical methods consistent with the experimental results. Huang et al. (2008) investigated the porosity change in spherical particles of various sizes using transparent soil experiments. Presently, the research on the failure mechanism of the interface mainly

focuses on shear failure and seepage failure. Shear failure is usually studied through direct shear tests. Potyondy (1961) conducted interface friction tests with soil and various building materials; Desai, Drumm, and Zaman (1985) conducted direct shear tests on the soil-concrete interface and proposed a new stress-strain model. Seepage failure is usually studied through soil permeability experiments. Xie et al. (2018) analyzed the factors affecting the critical hydraulic gradient at the soil-structure interface through experiments. They found that higher compactness and clay content led to a higher critical hydraulic gradient, and interface roughness initially increased and then decreased the critical hydraulic gradient. Chen et al. (2022) discovered in their experiments that soil particles at the rough contact surface were looser, making interface erosion more likely to occur.

Previous studies on the soil-structure interface have mainly focused on the interface itself while neglecting the differences in structure and seepage properties between the soil on the interface and the internal soil. Investigating these differences is crucial to comprehending and preventing soil failure on the interface. However, it is difficult to observe the internal soil with conventional soil. At present, there are many classic methods to visualize the internal structure of the soil, such as scanning electron microscopy (SEM) (Feng et al. 2019), transmission electron microscopy (TEM) (G. H. Taylor, Liu, and Teichmüller 1991), and X-ray micro-computed tomography (micro-CT) (Yuan et al. 2022; H. F. Taylor, O'Sullivan, and Sim 2015). Compared with the above methods, the materials used in the transparent soil technology are more affordable. In addition, they can be combined with PIV to observe the fluid flow in the soil more intuitively. Therefore, transparent soil technology was used in this paper to study the structure and seepage characteristics of the internal soil.

The principle of transparent soil technology is to make the refractive index of soil and pore fluid consistent so that the interior of the soil can be directly observed. In the selection of experimental materials, solid particles mainly include fused silica sand, borosilicate glass, and organic glass; the selection of liquid in the experiment should meet four criteria: safe and healthy, no excessive volatilization, low viscosity, and affordable (Ezzein and Bathurst 2011). It is mainly divided into two categories: oil and inorganic aqueous solutions. As it is challenging to match the refractive index of fluids with that of solids, altering the refractive index of the fluid is necessary. Currently, there are two methods for modifying the liquid refractive index (Dai et al., 2022). One is to mix two oils with different refractive indexes, and the refractive index of the mixed liquid is between the two oils. The refractive index of the new liquid can be adjusted by controlling the mixing ratio; the second is to change the concentration of the inorganic aqueous solution. The greater the concentration, the higher the refractive index. Some scholars have studied the material and mechanical properties of transparent soil and found that it has similar properties to natural soil so that it can be used in geotechnical engineering experiments instead of natural soil (Ezzein and Bathurst 2011; Zhong et al. 2022). Due to its unique advantages in soil visualization, transparent soil technology has been widely used in various fields of geotechnical engineering, such as seepage flow (Sanvitale et al. 2021), landslide (Sui and Zheng 2018; C. Zhou, Ma, and Sui 2022), suffusion (Hunter and Bowman 2018; Gu et al. 2021), grouting (Jinyuan Liu, Gao, and Sui 2013), pile-soil interaction (D. Zhou and Zhang 2018; Yang et al. 2022), debris flow (Sanvitale, Bowman, and Cabrera 2021) and tunnel construction (He 2021). In addition, by combining with image analysis methods, transparent soil technology can also be applied to the study of unsaturated soil (Peters, Siemens, and Take 2011; Que et al. 2022).

2. Experiments

2.1. Experimental materials

In this experiment, fused quartz sand with a particle size of 4.75-6 mm was utilized as the soil particle, and a mineral oil mixture with a matching refractive index was used as the fluid. The mineral oils utilized were P-40 and P-55, manufactured by MORESCO Co., Ltd. of Japan and blended at a 3:4 ratio at 20°C. To maintain transparency, all experiments were conducted at a constant temperature of 20°C

In Fig. 2, there is only P-40 in the left container and mineral oil mixed at 3:4 in the right container. It can be seen that the fused quartz sand in the right container is very transparent.

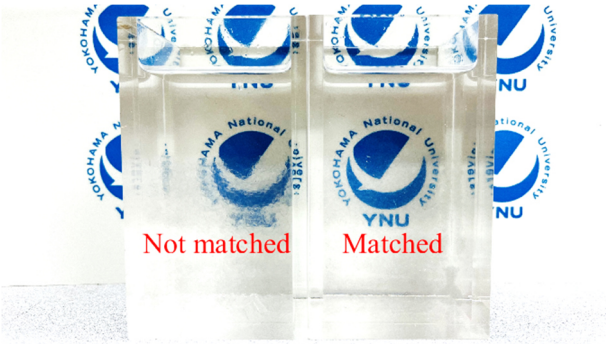

Figure 2. The mixture of fused quartz sand and mineral oil (The fluid in the left container is P-40, and the fluid in the right container is mineral oil mixed at 3:4).

2.2. Experimental setup

Fig. 3 depicts the experimental setup, with ⓐ is the fluid supply box; ⓑ is a green laser with a wavelength of 532 nm; ⓒ is a high-speed camera equipped with a long-pass filter to eliminate scattered light, ⓓ is spherical glass beads employed to evenly distribute the fluid flow into the soil; ⓔ is the fused quartz sand; ⓕ is the seepage cell; ⓖ is the fluid collection tank, utilized to gather the mineral oil that exits the system; and ⓗ is the flowmeter, utilized to measure the flow velocity throughout the experiments.

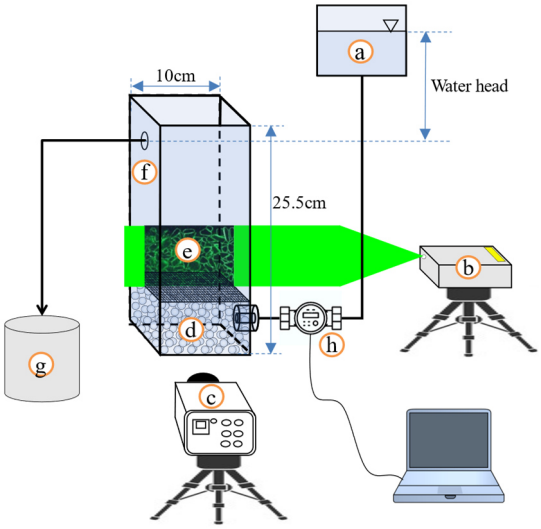

Figure 3. Experimental setup.

2.3. Experimental procedure

In the experiment, fused quartz sand with a particle size of 4.75-6 mm was used to carry out the permeability experiment under different relative densities. The relative densities were 60%, 80%, and 95%, respectively, and the hydraulic gradient was fixed at 0.5. To ensure the repeatability of the experiment, two experiments were conducted for each relative density. Table 1 shows the basic data of three soil samples with different relative densities.

Table 1. Basic data of soil samples

Relative density	Density (g/cm^3)	Porosity
60%	1.269	42.39%
80%	1.307	40.65%
95%	1.338	39.28%

Fig. 4 shows the transparent soil in the experiment. The objects behind the soil can be seen clearly by observing the pictures, which is enough to prove that it has high transparency. The soil material was divided into ten layers and then compacted to a specified density to obtain a homogeneous specimen. The size of the soil sample was 10 cm × 10 cm × 10 cm, and a rectangular black box measuring 5 cm × 4 cm was painted on it. Only the soil within the black box was observed each time to avoid the influence of different observation positions on the experimental results.

Figure 4. Transparent soil in the experiment.

Fig. 5 shows a working laser with a slide rail installed underneath it which can be used to adjust the position. The laser started from the side wall and moved to the internal soil, 30mm away from the side wall. The laser stayed for 6 seconds every 1mm. At the same time, the high-speed camera with an FPS of 100 was used to take continuous images. Six hundred photos were taken each time, a total of 31 times.

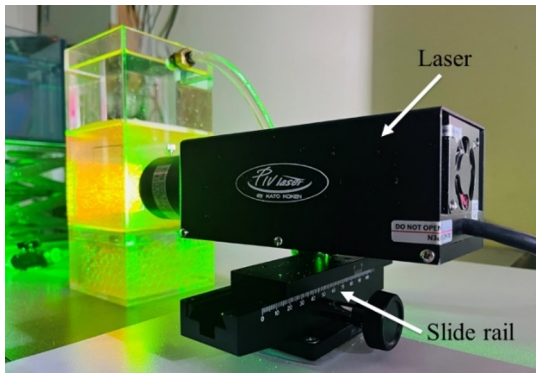

Figure 5. Laser with a slide rail.

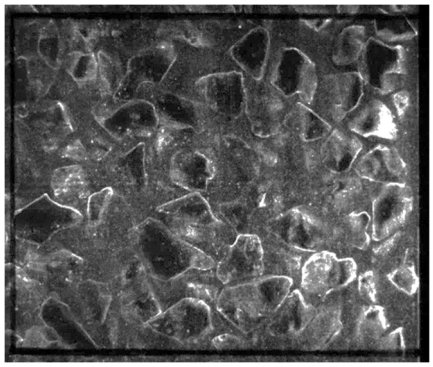

(1) 0 mm from the boundary

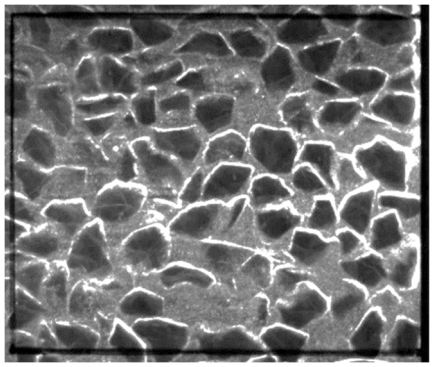

(2) 10 mm from the boundary

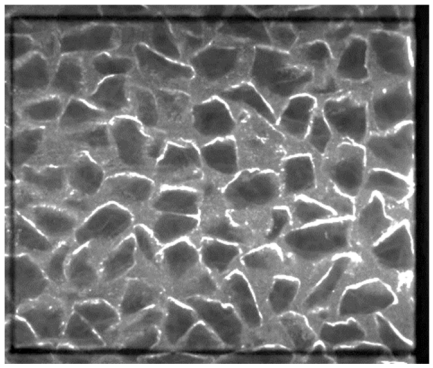

(3) 30 mm from the boundary

Figure 6. Original images.

3. Results and discussion

3.1. Porosity analysis

In order to analyze the porosity of soil through images, it is necessary to separate the soil particles and pores. First, the images were sharpened by Laplacian filtering in the commercial software Flownizer. Next, the brightness, contrast, and gamma value of the image were adjusted. These three values vary slightly for different photos, and finally, the maximum filtering was used to preliminarily separate the soil particles. Next, ImageJ was used to cut out the area in the black rectangular box and adjust the picture threshold to remove the spot in the middle of the particle and the black spot in the fluid to distinguish the particles and pores. Finally, the porosity was determined by calculating the area ratio of the black portion to the entire image. For example, the soil sample with a relative density of 60% was utilized. Fig. 6 displays the original images obtained from the experiment, and Fig. 7 displays the processed images.

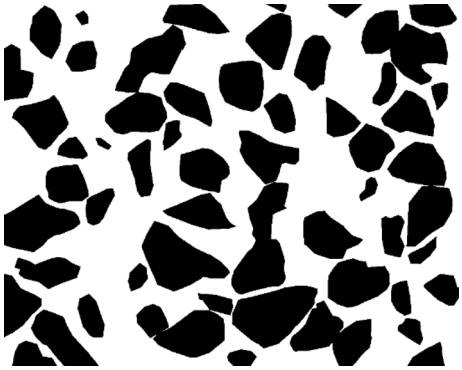

(1) 0 mm from the boundary

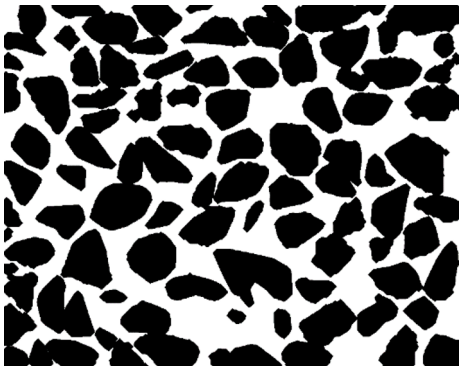

(2) 10 mm from the boundary

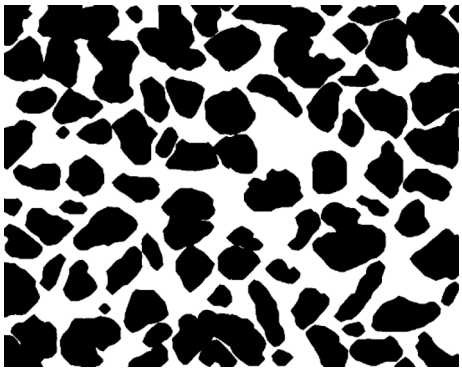

(3) 30 mm from the boundary

Figure 7. Processed images.

Fig. 8 illustrates the relationship between the porosity of soils with different relative densities and the distance from the side wall. As shown in the figure, the porosity of soils with any relative density reaches its maximum value at the soil-structure interface. In contrast, the porosity of the internal soil fluctuates around the average porosity (indicated by the red line in Fig. 8). The porosity at the interface is approximately 1.3 times greater than the overall porosity. It is also apparent from Figs. 6 and 7 that the porosity at the interface is larger. This is attributed to the barrier effect of the rigid side wall on soil particles, which results in only a small portion of soil particles being in contact with the side wall, thereby creating relatively large pores and porosity at the interface.

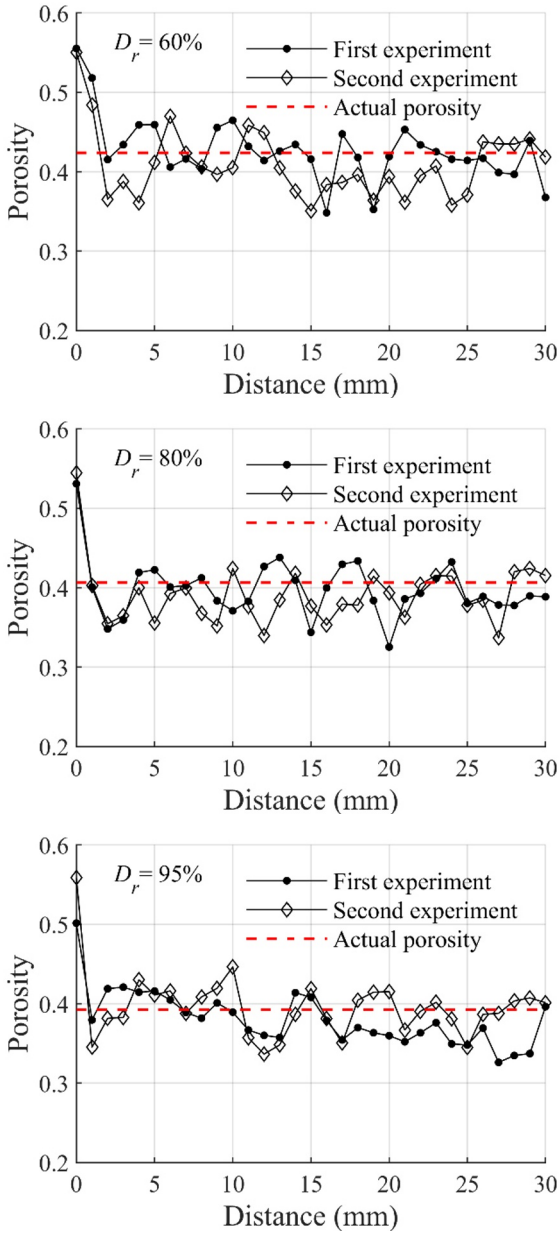

Figure 8. Relationship between the porosity of soils with different relative densities and distance from the side wall.

To investigate the relationship between soil porosity and distance from the soil-structure interface, many researchers have utilized spherical particles rather than

actual soil particles. Mueller (1997) employed four numerical models to examine the porosity variation of spherical particles of the same size. The results showed that the porosity of spherical particles reached its maximum at the interface, approximately 2.5 times higher than the average porosity. Huang et al. (2008) conducted a transparent soil experiment using spherical particles of different sizes. They observed that the porosity of spherical particles fluctuated regularly from the side wall to the interior, with a period of approximately the diameter of the spherical particles. The maximum porosity appeared at the soil-structure interface, about twice the average porosity. However, in this experiment, irregular particles were stacked to form soil, resulting in irregular changes in porosity, unlike the regular fluctuations observed in spherical particle experiments. Additionally, the ratio of maximum porosity to average porosity in this experiment was only 1.3, whereas, in experiments with spherical particles, it was more than 2. This disparity could be attributed to some irregular particles having a larger contact surface area with the side wall. In contrast, the contact area between spherical particles and the side wall is relatively small, resulting in a larger soil porosity near the wall formed by spherical particles.

3.2. Velocity distribution in soil

To obtain the flow velocity of the fluid in the soil, Particle Image Velocimetry (PIV) technology is used, which is a non-contact method for measuring instantaneous fluid velocity. This method uses auto-correlation or cross-correlation algorithms to obtain the most likely moving path of particles and then determine their velocity. In this experiment, PIVlab, an open-source software based on Matlab, is used to calculate the flow velocity field in the soil. The high-speed camera used in the experiment has a frame rate of 100 FPS, allowing for images to be taken every 0.01 seconds. The distance moved by particles between two adjacent images is calculated through PIV analysis. The instantaneous velocity between two images can be obtained using Eq. (1). To compare different working conditions, the average velocity over a period of 6 seconds is calculated using Eq. (2).

$$v_i = {}^{s_i}/_{\Delta t} \tag{1}$$

$$v = {}^{\sum v_i}/_{599} \tag{2}$$

where v_i is the velocity between two adjacent pictures, s_i is the distance between two adjacent pictures, Δt is the time interval, which is 0.01 s here, v is the average velocity between 6 s.

Fig. 9 shows the flow velocity field of the soil sample with a relative density of 60% at different distances from the side wall. It can be found that there are some long flow paths with large velocities on the boundary, indicating that the path flows along the side wall all the time, which is a two-dimensional flow. However, the flow path of high velocity in the soil is usually short, which indicates that the fluid leaves the current plane along the edge of soil particles, so the flow in the soil is three-dimensional.

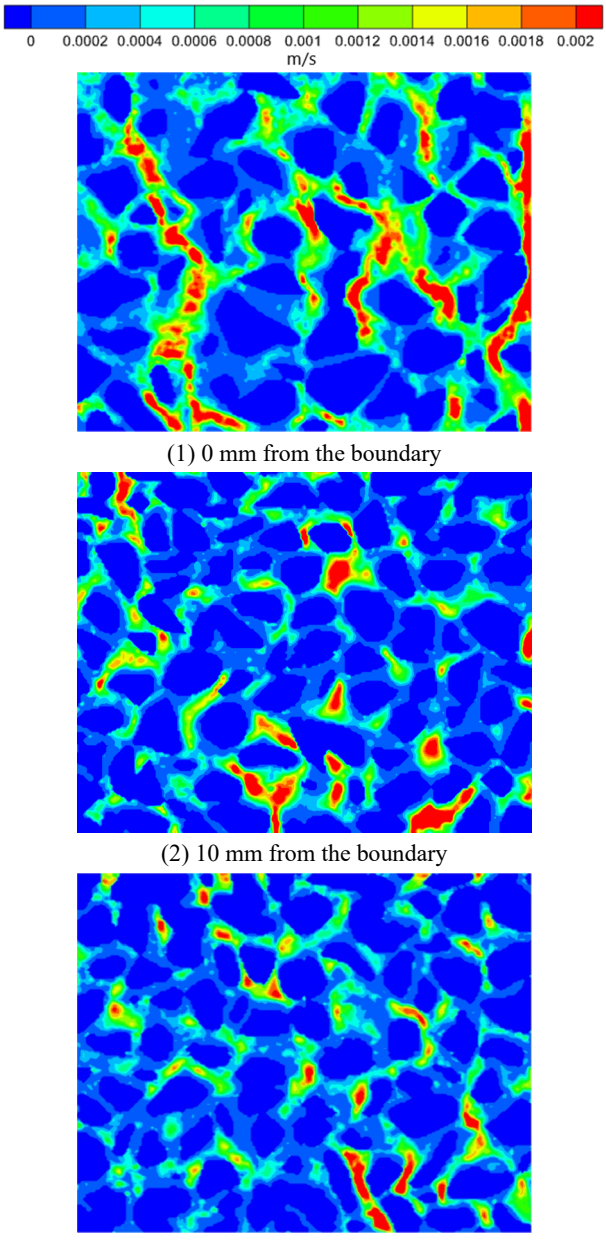

(1) 0 mm from the boundary

(2) 10 mm from the boundary

(3) 30 mm from the boundary

Figure 9. Flow velocity flied.

Fig. 10 depicts the relationship between the average velocity of soil with different relative densities and the distance from the interfaces. The average velocity is calculated using Eq. (2). It is observed that the maximum value of the average velocity of soil with any relative density occurs where the soil contacts the side wall, referred to as the dominant flow phenomenon. This is due to the presence of macropores at the soil-wall interface, where the fluid flows vertically upwards along the side wall, resulting in flow occurring only in the plane of the side wall. On the other hand, the fluid in the soil flows upwards along the edge of the soil particles, which is not in the same plane, thus leading to a higher average velocity at the soil-structure interface.

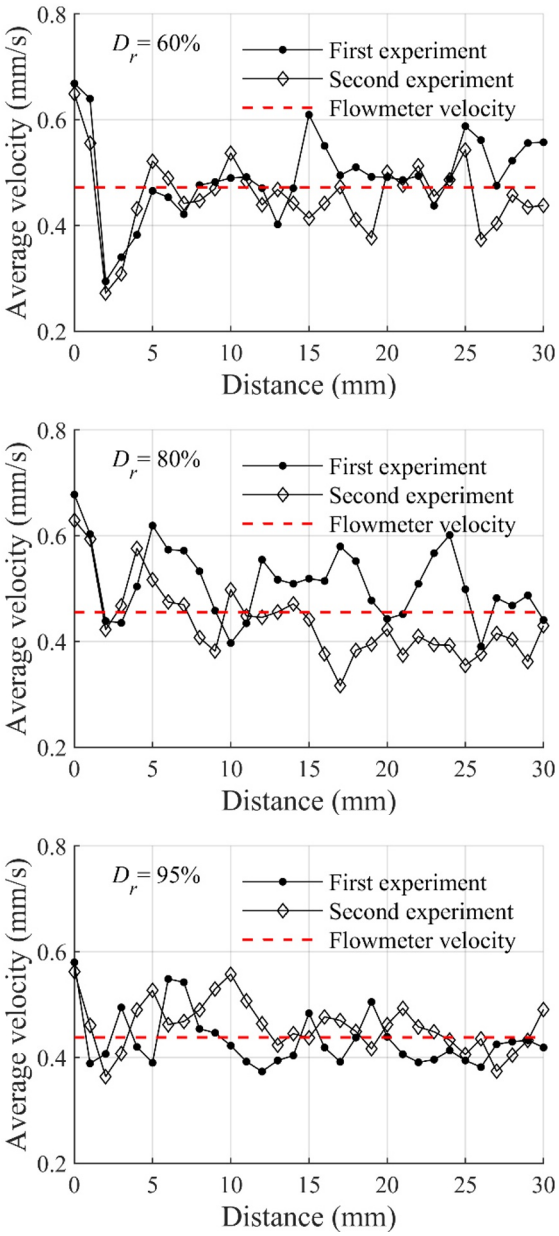

Figure 10. Relationship between the average velocity and the distance between the interfaces

4. Conclusion

In this paper, permeability experiments were conducted on different relative densities using transparent soil technology. The porosity and flow velocity field in the soil were obtained through image analysis, and the differences between the soil-structure interface and the soil interior were studied through porosities and average velocities at different locations. The main conclusions are as follows:

(1) The rigid sidewall acts as a barrier to soil particles, resulting in most particles having minimal contact with the wall. This creates large pores at the soil-structure interface, leading to higher porosity in this region compared to the interior of the soil. Specifically, the porosity at the interface is approximately 1.3 times higher than inside the soil.

(2) The fluid's average velocity varies on different slices, reaching its maximum at the soil-structure interface. This is due to the presence of large pores along the rigid side wall, which allow high-velocity flow paths to move vertically along the wall and always remain in the same plane. However, inside the soil, the flow paths move upward along the edge of the soil particles, and the high-velocity paths eventually move out of the current plane after some distance. As a result, the average velocity on the slice inside the soil is negligible.

References

Chen, Chenghao, Shiang Mei, Shengshui Chen, Yi Tang, and Chengwei Wan. 2022. "Laboratory Investigation of Erosion Behavior at the Soil–Structure Interface Affected by Various Structural Factors." *Natural Hazards* 111 (1): 1065–84. https://doi.org/10.1007/s11069-021-05070-4

Dai, Xu, Lei He, Wuxing Wu, and Jian Chen. 2022. "Visualization Experiment Technology Based on Transparent Geotechnical Materials and Its Engineering Application." *Journal of Visualization*. https://doi.org/10.1007/s12650-022-00863-6

Desai, C. S., E. C. Drumm, and M. M. Zaman. 1985. "Cyclic Testing and Modeling of Interfaces." *Journal of Geotechnical Engineering* 111 (6): 793–815. https://doi.org/10.1061/(ASCE)0733-9410(1985)111:6(793)

Ezzein, Fawzy M., and Richard J. Bathurst. 2011. "A Transparent Sand for Geotechnical Laboratory Modeling." *Geotechnical Testing Journal* 34 (6): 1–12. https://doi.org/10.1520/GTJ103808

Feng, Huaiping, Deliang Ma, Qiyuan Liu, and Chaoliang Ye. 2019. "Method for Calculating Three Dimensional Apparent Porosity of Soils Based on SEM Images." *Chinese Journal of Geotechnical Engineering* 41 (3): 574–80. https://doi.org/10.11779/CJGE201903021

Gu, Jingyun, Yulong Luo, Xingjie Zhang, Meili Zhan, Yuan Wang, and Jinchang Sheng. 2021. "A Suffusion Visualization Apparatus Based on Planar Laser Induced Fluorescence and the Preliminary Application." *Chinese Journal of Rock Mechanics and Engineering* 40 (6). https://doi.org/10.13722/j.cnki.jrme.2020.0740

He, Lei. 2021. "Study on Soil Deformation Induced by Double-O-Tube Shield Tunnel Construction Based on Transparent Soil Technology." Chongqing Jiaotong University.

Huang, Alice Y.L., Michelle Y.F. Huang, Hervé Capart, and Rong Her Chen. 2008. "Optical Measurements of Pore Geometry and Fluid Velocity in a Bed of Irregularly Packed Spheres." *Experiments in Fluids* 45 (2): 309–21. https://doi.org/10.1007/s00348-008-0480-x

Hunter, R. P., and Elisabeth Bowman. 2018. "Visualisation of Seepage-Induced Suffusion and Suffosion within Internally Erodible Granular Media." *Geotechnique* 68 (10): 918–30. https://doi.org/10.1680/jgeot.17.P.161.

Independent panel to review cause of Teton dam failure. 1976. "Report to U.S. Department of the Interior and State of Idaho on Failure of Teton Dam."

Liu, Jie. 2004. "Analysis of Dam Break of Bayi Reservoir." *Journal of China Institute of Water Resources and Hydropower Research* 2 (3): 161–66. https://doi.org/10.13244/j.cnki.jiwhr.2004.03.001

Liu, Jinyuan, Yue Gao, and Wanghua Sui. 2013. "Visualization of Grout Permeation inside Transparent Soil." In *Second International Conference on Geotechnical and Earthquake Engineering*, 188–94. Chengdu, China.

Luo, Yulong, Meili Zhan, Jinchang Sheng, and Qiang Wu. 2013. "Hydro-Mechanical Coupling Mechanism on Joint of Clay Core-Wall and Concrete Cut-off Wall." *Journal of Central South University* 20 (9): 2578–85. https://doi.org/10.1007/s11771-013-1771-9

Mueller, Gary E. 1992. "Radial Void Fraction Distributions in

Randomly Packed Fixed Beds of Uniformly Sized Spheres in Cylindrical Containers." *Powder Technology* 72 (3): 269–75. https://doi.org/10.1016/0032-5910(92)80045-X

Mueller, Gary E. 1997. "Numerical Simulation of Packed Beds with Monosized Spheres in Cylindrical Containers." *Powder Technology* 92 (2): 179–83. https://doi.org/10.1016/S0032-5910(97)03207-5

Peters, S. B., G. Siemens, and W. A. Take. 2011. "Characterization of Transparent Soil for Unsaturated Applications." *Geotechnical Testing Journal* 34 (5): 445–56. https://doi.org/10.1520/GTJ103580

Potyondy, J.G. 1961. "Skin Friction Between Various Soils and Construction Materials." *Geotechnique* 11 (4): 339–53. https://doi.org/10.1680/geot.1961.11.4.339

Que, Yun, Bin Weng, Songlin Cai, and Jinyuan Liu. 2022. "Analysis of Preferential Flow Migration in Unsaturated Transparent Soil." *Rock and Soil Mechanics* 43 (4): 857–67, 878. https://doi.org/10.16285/j.rsm.2021.1087

Ru, Naihua, and Yunguang Niu. 2001. *Embankment Dam—Incidents and Safety of Large Dams*. 1st ed. Beijing: China Water&Power Press.

Sanvitale, Nicoletta, Elisabeth Bowman, and Miguel Angel Cabrera. 2021. "Experimental Investigation on the Impact Dynamics of Saturated Granular Flows on Rigid Barriers." *Environmental and Engineering Geoscience* 27 (1): 127–38. https://doi.org/10.2113/EEG-D-20-00033

Sanvitale, Nicoletta, B. D. Zhao, Elisabeth Bowman, and C. O'Sullivan. 2021. "Particle-Scale Observation of Seepage Flow in Granular Soils Using PIV and CFD." *Geotechnique*, 1–18. https://doi.org/10.1680/jgeot.20.p.432

Sui, Wanghua, and Guosheng Zheng. 2018. "An Experimental Investigation on Slope Stability under Drawdown Conditions Using Transparent Soils." *Bulletin of Engineering Geology and the Environment* 77 (3): 977–85. https://doi.org/10.1007/s10064-017-1082-8

Taylor, Geoff H., Susie Y. Liu, and Marlies Teichmüller. 1991. “Bituminite - A TEM View.” *International Journal of Coal Geology* 18 (1–2): 71–85. https://doi.org/10.1016/0166-5162(91)90044-J

Taylor, H. F., C. O'Sullivan, and W. W. Sim. 2015. "A New Method to Identify Void Constrictions in Micro-CT Images of Sand." *Computers and Geotechnics* 69: 279–90. https://doi.org/10.1016/j.compgeo.2015.05.012

Thielicke, William, and Eize J. Stamhuis. 2014. "PIVlab – Towards User-Friendly, Affordable and Accurate Digital Particle Image Velocimetry in MATLAB." *Journal of Open Research Software* 2. https://doi.org/10.5334/jors.bl

Xie, Quanyi, Jian Liu, Bo Han, Hongtao Li, Yuying Li, and Xuanzheng Li. 2018. "Critical Hydraulic Gradient of Internal Erosion at the Soil-Structure Interface." *Processes* 6 (7). https://doi.org/10.3390/PR6070092

Yang, Qingnian, Jianli Shao, Zhijun Xu, and Yu Miao. 2022. "Experimental Investigation of the Impact of Necking Position on Pile Capacity Assisted with Transparent Soil Technology." *Advances in Civil Engineering* 2022: 1–10. https://doi.org/10.1155/2022/9965974

Yuan, Shengyang, Xianfeng Liu, Yongxing Wang, Pierre Delage, Patrick Aimedieu, and Olivier Buzzi. 2022. "X-Ray Microtomography of Mercury Intruded Compacted Clay: An Insight into the Geometry of Macropores." *Applied Clay Science* 227 (June): 106573. https://doi.org/10.1016/j.clay.2022.106573

Zhong, Wenhan, Hanlong Liu, Dongming Gu, Wengang Zhang, Chao Yang, and Xuecheng Gao. 2022. "Development of a Preparation Method of Transparent Soil-Rock Mixture for Geotechnical Laboratory Modeling." *Engineering Geology* 301 (February 2021): 106622. https://doi.org/10.1016/j.enggeo.2022.106622

Zhou, Chang, Wenchao Ma, and Wanghua Sui. 2022. "Transparent Soil Model Test of a Landslide with Umbrella-Shaped Anchors and Different Slope Angles in Response to Rapid Drawdown." *Engineering Geology* 307 (December 2021): 106765. https://doi.org/10.1016/j.enggeo.2022.106765

Zhou, Dong, and Wengang Zhang. 2018. "Transparent Soil Model Test on Displacement Field of Soils around Single Passive Pile." In *International Conference on Geotechnical and Earthquake Engineering 2018*, 652–59. Chongqing, China.